Molecular Therapy
Oncolytics
Original Article

AMERICAN SOCIETY of GENE & CELL THERAPY

Dual-Isotope SPECT Imaging with NIS Reporter Gene and Duramycin to Visualize Tumor Susceptibility to Oncolytic Virus Infection

Lianwen Zhang,[1,5] Lukkana Suksanpaisan,[2,5] Huailei Jiang,[3] Timothy R. DeGrado,[3] Stephen J. Russell,[1] Ming Zhao,[4] and Kah-Whye Peng[1]

[1]Department of Molecular Medicine, Mayo Clinic, Rochester, MN, USA; [2]Imanis Life Sciences, Rochester, MN, USA; [3]Department of Radiology, Mayo Clinic, Rochester, MN, USA; [4]Northwestern University, Chicago, IL, USA

Noninvasive dual-imaging methods that provide an early readout on tumor permissiveness to virus infection and tumor cell death could be valuable in optimizing development of oncolytic virotherapies. Here, we have used the sodium iodide symporter (NIS) and ^{125}I radiotracer to detect infection and replicative spread of an oncolytic vesicular stomatitis virus (VSV) in VSV-susceptible (MPC-11 tumor) versus VSV-resistant (CT26 tumor) tumors in BALB/c mice. In conjunction, tumor cell death was imaged simultaneously using technetium (^{99m}Tc)-duramycin that binds phosphatidylethanolamine in apoptotic and necrotic cells. Dual-isotope single-photon emission computed tomography/computed tomography (SPECT/CT) imaging showed areas of virus infection (NIS and ^{125}I), which overlapped well with areas of tumor cell death (^{99m}Tc-duramycin imaging) in susceptible tumors. Multiple infectious foci arose early in MPC-11 tumors, which rapidly expanded throughout the tumor parenchyma over time. There was a dose-dependent increase in numbers of infectious centers and ^{99m}Tc-duramycin-positive areas with viral dose. In contrast, NIS or duramycin signals were minimal in VSV-resistant CT26 tumors. Combinatorial use of NIS and ^{99m}Tc-duramycin SPECT imaging for simultaneous monitoring of oncolytic virotherapy (OV) spread and the presence or absence of treatment-associated cell death could be useful to guide development of combination treatment strategies to enhance therapeutic outcome.

INTRODUCTION

Oncolytic virotherapy (OV) is a promising new class of anticancer modality under development for a variety of cancers.[1,2] Oncolytic virotherapy uses recombinant replication-competent viruses that have been genetically engineered for enhanced immune activation and tumor-selective replication.[3,4] Viruses from diverse families have demonstrated substantial efficacy in preclinical models and are being assessed in various clinical trials.[5] In addition to OV-mediated tumor killing by direct infection, the release of tumor-associated antigens subsequent to viral-induced cell killing/death initiates a pro-inflammatory response, which promotes systemic antitumor immunity.[3,6,7] Accordingly, OV exposure may promote immediate and lasting anticancer effects, making it a highly attractive modality to combine in immuno-oncology drugs against a broad spectrum of cancers.[8,9]

Vesicular stomatitis virus (VSV), from the family *Rhabdoviridae*, is a promising oncolytic virus under investigation in preclinical studies and in clinical trials.[10,11] VSV is an effective anticancer vector platform due to a variety of key features: (1) VSV has rapid replication kinetics and high burst size; (2) low sero-prevalence allowing intravenous administration; and, importantly; and (3) can be genetically engineered to encode transgenes to improve specificity and potency.[11] Previous strategies used in modulating VSV include the incorporation of the interferon β (IFNβ) gene into the VSV genome to enhance tumor selectivity and potentiate immune-mediated antitumor activity.[12] In addition to genetic modifications used to achieve maximal tumor infection and oncolytic effects, VSVs encoding reporter genes can provide an early readout during preclinical studies. The sodium iodide symporter (NIS) is a self-protein expressed endogenously in the thyroid for the uptake of iodine for the synthesis of thyroid hormones.[13] As such, NIS is used clinically in conjunction with ^{123}I gamma camera imaging for the diagnosis of thyroid disorders and treatment of metastatic thyroid cancer using beta-emitting ^{131}I. Our group has previously engineered VSV to encode NIS, which enables noninvasive, longitudinal monitoring of pharmacokinetic activity and viral invasion of tumors when visualized via single-photon emission computed tomography (SPECT/CT).[9,14,15] Furthermore, NIS can enable noninvasive tracking of pharmacokinetic activity relating to viral infection and expression, target validation, and susceptibility of specific tumor types.[15] In a phase I clinical trial using a measles virus (MV) encoding NIS (MV-NIS) in patients with multiple myeloma, we demonstrated the utility and significance of the NIS reporter gene in tracking MV infection in plasmacytomas in patients over time.[8,16] SPECT/CT also can precisely measure the degree of

Received 22 August 2019; accepted 5 October 2019;
https://doi.org/10.1016/j.omto.2019.10.002.

[5]These authors contributed equally to this work.

Correspondence: Kah-Whye Peng, Department of Molecular Medicine, Mayo Clinic, 200 First Street SW, Rochester, MN 55905, USA.
E-mail: peng.kah@mayo.edu

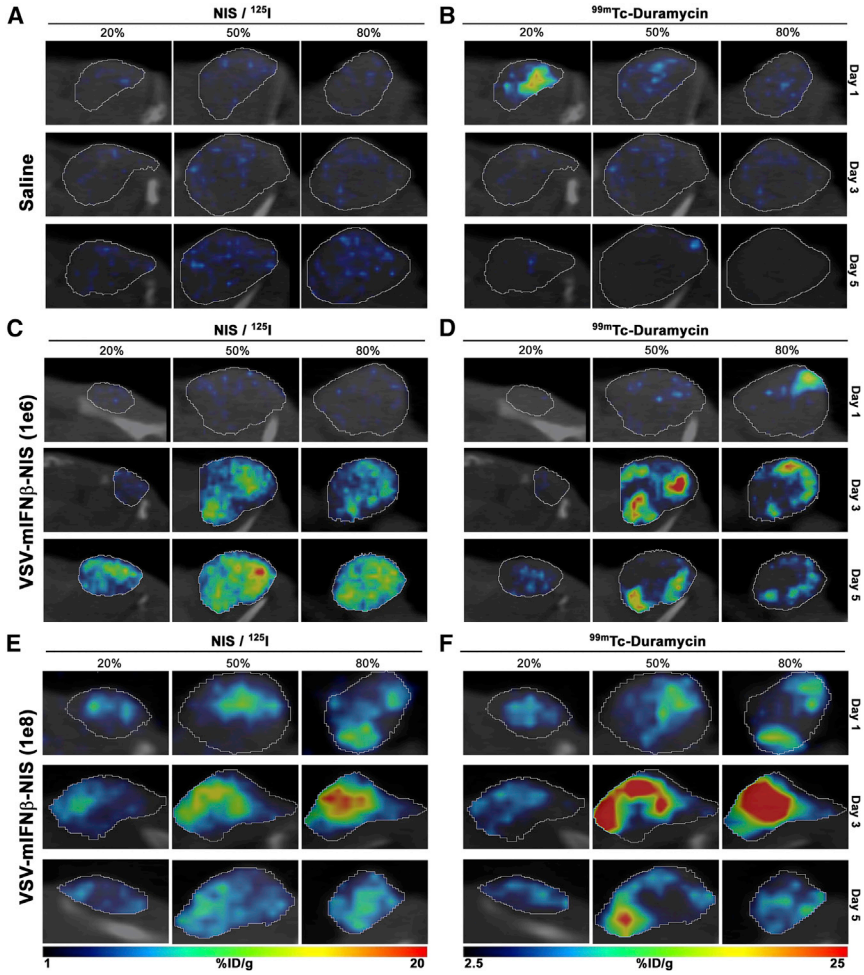

Figure 1. Intratumoral Spread and Dose-Dependent Response after Intravenous Administration of VSV-mIFNβ-NIS Virus in BALB/c Mice with MPC-11 Tumors

(A–F) Representative fused images of tumors. Saline controls (A and B) and BALB/c mice administered with VSV-mIFNβ-NIS at a dose of 10^6 $TCID_{50}$ (C and D) or 10^8 $TCID_{50}$ (E and F) were imaged by SPECT on days 1, 3, and 5 following virus treatment. Relative viral infectivity is measured as a function of VSV-mIFNβ-NIS-mediated ^{125}I uptake as shown in the left column (A, C, and E), and cell killing is measured by ^{99m}Tc-duramycin radiotracer activity as shown in the right column (B, D, and F). Percentage in figure indicates fractions of the entire tumor diameter.

viral-mediated cell killing and oncolytic potency by using ^{99m}Tc-duramycin as a radiotracer molecule. Indeed, ^{99m}Tc-duramycin is well characterized as a radiopharmaceutical and can serve as a highly sensitive molecular probe that binds phosphatidylethanolamine (PTE) molecules.[17] Because PTE is translocated en masse from inner to outer plasma membranes during the early stages of apoptosis, ^{99m}Tc-duramycin could be used in conjunction with SPECT imaging to detect apoptotic or necrotic cells.[18] Using this combinatorial approach of VSV and duramycin, we wanted to determine whether the methodology is sensitive enough for us to simultaneously track virus infection and monitor oncolytic potency while observing any off-target infection. If successful, this methodology could be particularly useful in combination studies whereby drugs and radioisotopes are added in combination with virus to enhance efficacy.[14,19]

RESULTS

Imaging Kinetics of VSV Infection in Murine Tumors

Here, we used a mouse myeloma MPC-11 tumor model that is known to be highly susceptible to VSV infection for these studies.[20,21] Whole-body imaging showed only physiologic uptake of ^{125}I due to endogenous NIS expression in the thyroid, salivary glands, and stomach, and no significant off-target infection by a recombinant VSV encoding murine IFNβ (mIFNβ) and human NIS (VSV-mIFNβ-NIS) in BALB/c mice (data not shown).[9] Representative fused SPECT/CT images of MPC-11 flank tumors in mice given saline, 10^6 (low-dose group) 50% tissue culture infective dose ($TCID_{50}$), or 10^8 $TCID_{50}$ (high-dose group) VSV-mIFNβ-NIS are shown in Figure 1. Imaging scans were performed on days 1 (24 h), 3, and 5 post VSV administration. NIS-positive signals were detectable in virus-treated mice, but not in saline-treated animals. No infectious foci were seen at day 1 in mice given 10^6 $TCID_{50}$ virus, whereas numerous infectious foci were detected in tumors from mice that received 10^8 $TCID_{50}$ virus, indicating an initial dose-dependent viral delivery and spread. Mice treated with low-dose virus showed increasing numbers of ^{125}I NIS-positive foci over the course of 5 days. Signals were highest at day 3 in the 10^8 $TCID_{50}$ group, followed by a decrease by day 5, potentially because of death of the infected cells (Figure 1E). These imaging data reveal a difference in initial viral infection and subsequent intratumoral spread between the low- and high-dose groups, and underscore the importance of efficient virus delivery and infection in achieving maximal tumor infectivity. In contrast, SPECT/CT imaging for NIS activity was negative in CT26 tumors, which are known to be resistant to VSV-mIFNβ-NIS therapy (Figures 2A and 2C).[22]

Imaging Tumor Cell Killing Using ^{99m}Tc-Duramycin

In addition to giving mice ^{125}I for NIS imaging, we co-administered ^{99m}Tc-duramycin that binds to PTE exposed on apoptotic cells and performed dual-isotope SPECT scans. As shown in Figure 1B, the MPC-11 tumor was negative for duramycin uptake in saline-treated mice, although some signal-positive areas were seen, likely because of a central region of necrosis in the tumor.

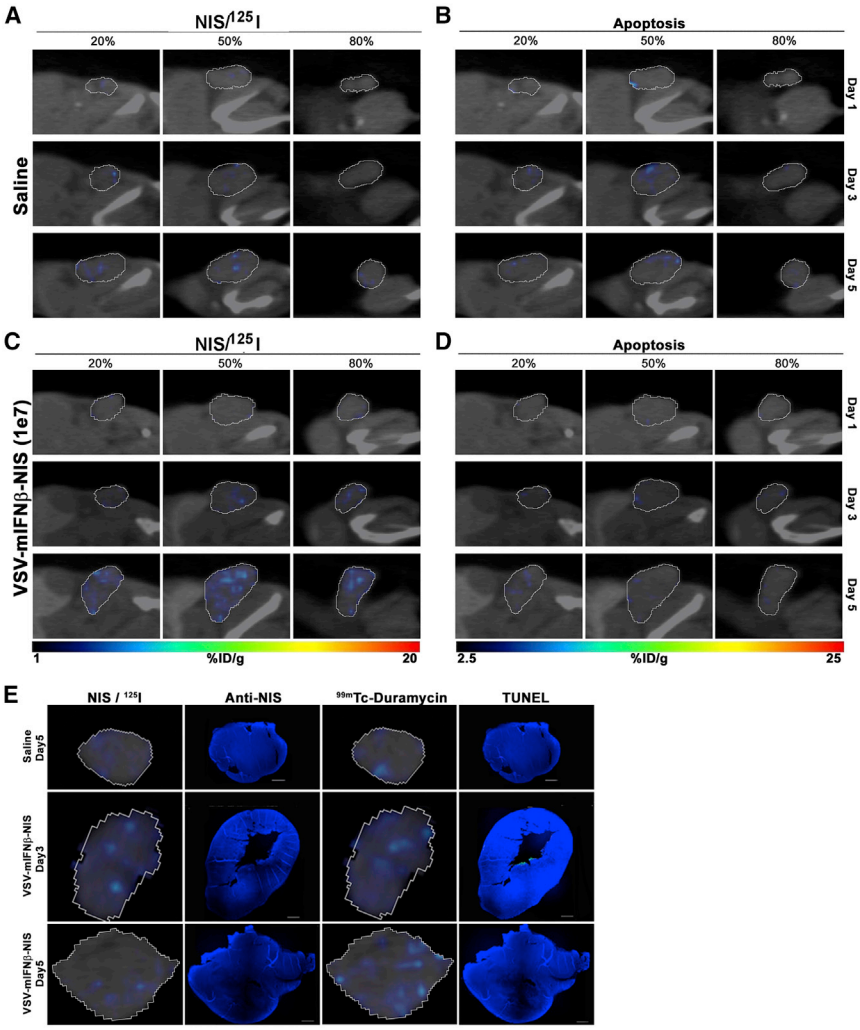

Figure 2. Intratumoral Spread of VSV-mIFNβ-NIS Virus after Intravenous Administration into BALB/c Mice with CT-26 Tumors

(A–D) Mice treated with saline (A and B) or VSV-mIFNβ-NIS at 10^7 $TCID_{50}$ (C and D) were imaged by SPECT on days 1, 3, and 5 following virus delivery. Relative viral infectivity is measured as a function of VSV-mIFNβ-NIS-mediated ^{125}I uptake as shown in the left column (A and C), and cell killing is measured by ^{99m}Tc-duramycin radiotracer activity as shown in the right column (B and D). Percentage in figure indicates fractions of the entire tumor diameter. (E) IHC stained tumor sections showing minimal positivity for NIS protein or apoptotic cells (TUNEL).

In both low- and high-dose VSV groups, significant ^{99m}Tc-duramycin signals were detected. These areas of cell killing overlap very well with areas of NIS expression in the VSV-infected foci, confirming that in VSV-responsive tumors, virus-infected cells rapidly die of the oncolytic effect from day 1 (Figures 1E and 1F). Because the NIS-positive foci increased intratumorally over several days, there was a corresponding progressive increase in duramycin-labeled areas in the tumors. The rapid increase of duramycin signals also indicates that VSV infection rapidly induces apoptosis in the infected cells, and concurs with previous studies showing significant increase in caspase-8 activity in infected cells at 8 h postinfection.[23] In contrast, minimal duramycin-positive areas were seen in the CT26 VSV-treated tumors (Figures 2B and 2D).

Immunofluorescence Staining Confirmed ^{125}I SPECT Imaging

To confirm that positive signals from ^{125}I SPECT imaging correlate with VSV infection, we harvested tumors at days 3 and 5 immediately after SPECT imaging and stained the tumor tissues for VSV antigen, NIS protein, or TUNEL assay (Figure 3). ^{125}I SPECT data at a specific slice of the tumor (radiohistology) showed increase in coverage of tumor by NIS-expressing cells over the 5 days (Figure 3A). Immunohistochemical (IHC) staining confirmed these areas expressed VSV and NIS antigens, indicating that the ^{125}I signals were indeed due to VSV-mIFNβ-NIS infection (Figures 3B and 3C). In parallel, we also focused on a specific slice from the SPECT data to identify areas of ^{99m}Tc-duramycin positivity (Figure 3D). There is a good correlation between duramycin-labeled areas from the SPECT imaging with DNA damage detected by TUNEL assay (Figure 3E). We also performed IHC staining of CT26 tumors, which showed minimal NIS-positive areas or duramycin uptake. Indeed, IHC staining did not show detectable levels of NIS antigen expression or TUNEL positivity (Figure 2E).

Space-Filling Models More Accurately Reflect the Distribution of Intratumoral Infection

As shown in Figure 3, TUNEL staining overlaps well with VSV and NIS staining, indicating VSV amplification is followed rapidly by tumor cell killing in these susceptible MPC-11 tumors. The SPECT imaging data can be rendered into 3D model space-filling models to facilitate better visualization of the 3D tomographic data (Figure 4). The 3D space-filling models allow us to combine all planar micro-SPECT/CT images into a comprehensive volume rendering of intratumoral infection distribution to help us gain a better spatial context and to visualize distributive relationships between these infectious centers (Figure 4; Video S1). Here, we can clearly see that there is a good concordance of the duramycin (red) and VSV activity (yellow) in the MPC-11 tumor from mice given an intravenous (i.v.) dose of VSV-mIFNβ-NIS virus. As expected, the NIS signals cover a larger

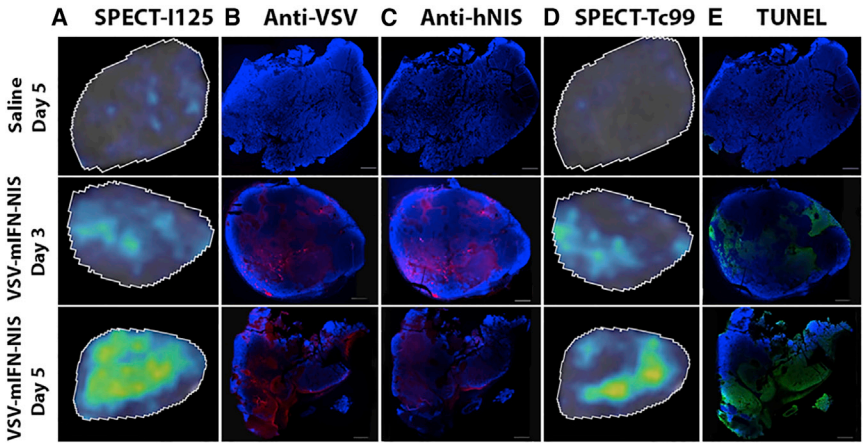

Figure 3. Correlating SPECT Imaging Data with Protein Expression (VSV and NIS Staining) or Cell Killing (TUNEL Staining for DNA Damage) in Tumor Sections

(A–E) MPC-11 tumors from BALB/c mice that received saline or 10^6 $TCID_{50}$ VSV-mIFNβ-NIS were harvested on days 3 and 5. Representative images of tumor sections are shown. (A–C) ^{125}I SPECT results at days 3 and 5 (A) are confirmed via IHC staining using anti-VSV antibody (B) and anti-hNIS antibody (C). (D and E) ^{99m}Tc SPECT results at days 3 and 5 (D) are confirmed using TUNEL assay (E).

volume of infection, and the apoptotic signals lag behind the VSV infection. The significance of this technology is evident when comparing conclusions made from IHC-stained tumor sections or planar microSPECT/CT images with the space-filling models. Whereas 2D slices do not provide contextual information and can misrepresent the extent of virus infection through the entire tumor, 3D space-filling models clearly demonstrate infection throughout the entire tumor.

Tumor Dosimetry Analysis Shows Parallel Trends between Virus Spread and Tumor Cell Killing

Region of interest (ROI) were drawn around the flank tumors in the SPECT images to determine the amount of radiotracer uptake in the tumors in the respective animals (Figure 4). In MPC-11 xenografts of mice (n = 4) treated with low-dose virus, there was a gradual increase in ^{125}I uptake over the course of 5 days (Figure 5A). Mean percentage uptake of injected dose per cubic centimeter of tissue (% ID/cm^3) is 1.08% ± 0.56% ID/cm^3 on day 1, increasing to 4.07% ± 1.42% ID/cm^3 on day 3 and 5.15% ± 2.76% ID/cm^3 on day 5. Mean uptake in mice (n = 4) in the high-dose group was 2.07% ± 0.36% ID/cm^3 on day 1, 2.73% ± 1.32% ID/cm^3 on day 3, followed by a steep decline in signal by day 5 (1.20% ± 0.16% ID/cm^3). Kinetics of tumor cell death, as measured by amount of ^{99m}Tc uptake, follows a similar trend to VSV infection in both low- and high-dose groups (Figure 5B). Conversely, CT26 xenografts showed a mean of 0.37% ± 0.37% ID/cm^3 over 5 days, confirming minimal viral infection in these tumors (Figure 5C).

DISCUSSION

We demonstrated here for the first time the feasibility of using ^{125}I and ^{99m}Tc dual-isotope imaging to simultaneously evaluate the replication of an oncolytic VSV and the corresponding viral-induced apoptotic cell death. ^{125}I emits low-energy photons of 35 keV with a 60-day physical half-life, and ^{99m}Tc emits photons with 140 keV and a 6-h physical half-life. For imaging dying infected cells, we used ^{99m}Tc-duramycin, which has a short half-life, has low background uptake by visceral organs, and has been proven to bind efficiently to apoptotic cells.[24–27] NIS reporter gene imaging is performed using ^{125}I, which has much lower energy at 35 keV and allows us to discriminate between the two profiles of the two isotopes to perform simultaneous imaging.

The areas of NIS-positive signals, a surrogate of viral replication, correlated well with the areas of duramycin signal that detect apoptotic/necrotic cells. Furthermore, the pharmacokinetics of viral gene expression and subsequent death of virally infected cells can be quantitated and followed for each single animal as frequently as desired by analysis of the SPECT data. Using longitudinal imaging, we detected increase in numbers of infectious foci over several days after initial viral infusion in MPC tumors that are highly responsive to VSV infection and killing. In MPC-11 mice given a low 10^6 $TCID_{50}$ i.v. dose of VSV, viral infection gradually builds up and peaked on day 5. There was a clear dose-dependence increase in initial viral extravasation and infectivity because NIS signals peaked more rapidly by day 3 in mice given 100-fold more virus, followed by decreasing uptake over the next few days of surveillance. In conjunction, ^{99m}Tc-duramycin uptake at day 2 was higher in mice treated with 10^8 $TCID_{50}$ VSV than with 10^6 $TCID_{50}$ VSV. From these dual-imaging data, we were able to conclude that response of MPC-11 tumor to VSV therapy is predominantly driven by initial oncolysis by the virus, resulting in rapid death of the cell.

Dual-isotope imaging that enables real-time tracking of viral replication and cell killing could facilitate understanding of mechanisms underlying therapy failure. Although this approach is likely to be costly and not easily adopted as standard of care in clinical practice, dual imaging could certainly help preclinical or early-phase clinical development of novel virus constructs and virus/drug combination studies. In contrast with MPC-11 tumors, CT26 tumors are resistant to VSV therapy.[28] Based on the imaging data, it is clear that treatment failure is due predominantly to the lack of significant viral infection of the tumor cells after viral delivery. *In vitro* studies showed that CT26 tumor cells are IFN responsive and are thus likely to have rapidly mounted a robust antiviral response after initial infection through

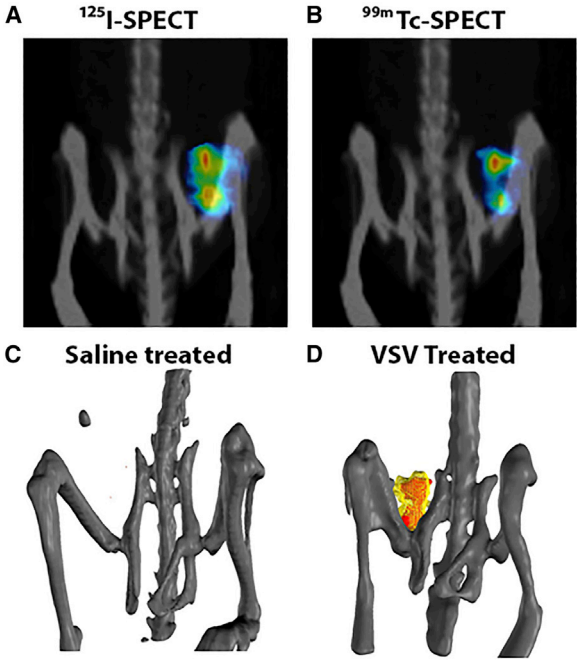

Figure 4. Three-Dimensional (3D) Space-Filled Rendering of SPECT/CT Tomographic Data Showing the Intratumoral Distribution of Viral Infection
(A and B) Maximal intensity projection images showing ^{125}I uptake in areas of VSV infection (A) and ^{99m}Tc uptake in areas of tumor cell death (B) in MPC-11 tumor at day 2. (C and D) 3D space-filling models of saline-treated mouse (C) and VSV-treated mouse (D); VSV infection (^{125}I uptake) is yellow, and apoptotic cells (^{99}Tc-duramycin uptake) are red.

activation of the type I IFN response pathway.[28] Studies have shown that addition of Jak1 inhibitors such as ruxolitinib could have a positive impact on IFN-responsive tumors by dampening the initial innate defense.[29–31] In another scenario, tumor cells that are permissive to viral infection (thus NIS-positive through SPECT imaging) but resistant to apoptosis would show low/negligible duramycin binding. In these tumors with high NIS expression and limited cell death, a timely dose of beta-emitting ^{131}I could potentially enhance virotherapy killing to boost cell killing as previously shown using a NIS-encoding VSV or MV.[14,19]

The positive viral imaging data in this study were confirmed by IHC staining for VSV antigen and NIS expression, confirming that the ^{125}I uptake was indeed due to VSV-infected cells expressing NIS. In contrast with invasive and time-consuming protocols such as IHC staining, SPECT imaging is noninvasive and allows the investigator to monitor the same living animal longitudinally over a desired time period. This not only reduces animal waste but also provides a more refined and superior dataset that includes tomographic data with spatial information on relative distribution of the infectious foci and its changes over time. Instead of simply obtaining a snapshot of the tumor in two dimensions, viral infection and cell death in the entire tumor can be easily captured and rendered. The data are not only qualitative, but quantitative. Drawing ROI around the flank tumor allows us to measure accurately the amount of radiotracer uptake over time per gram of tumor. These measurements indicate that for high-dose VSV, viral infection peaked at day 3 and declined thereafter. Indeed, viral replication kinetics demonstrated in this study concurred with previous studies where infectious virus recovery from tumor showed that VSV replication reached a peak by days 2–4, followed by a sharp decrease in activity by day 5, supporting our observations presented here.[20]

Reporter gene imaging for virus and cell tracking is often performed in rodents using bioluminescent imaging.[32,33] Bioluminescent imaging offers high-throughput screening and sensitivity, and is acceptable for routine studies. However, it lacks resolution and for studies as described in this work where we are tracking distribution of infectious foci, bioluminescent imaging would not be feasible because optical imaging lacks spatial resolution and is also negatively impacted by attenuation of photons from tissues more than a few millimeters deep.[34] It is ironic that although there are abundant preclinical studies developing therapies using bioluminescent imaging *in vivo*, investigators fail to incorporate these imaging studies during clinical development, where it perhaps matters most. In addition to NIS and duramycin imaging, there are other imaging modalities, e.g., magnetic resonance reporter gene imaging, which could be incorporated and are compatible clinically.[35] The majority of oncolytic viruses in clinical trials do not encode a reporter gene, except for GL-ONC1 (encodes Ruc-GFP, β-glucuronidase, and β-galactosidase genes), MV-NIS, and VSV-IFNβ-NIS (symporter/transport proteins [hNIS]). Using NIS imaging, authors were able to demonstrate delivery of virus to metastatic tumor deposits after intravenous administration of MV-NIS in myeloma patients.[8] Viral infection was seen between days 8 and 15, followed by subsequent clearance of NIS-infected cells by day 23.[8] In another study, Eidenschink et al.[36] have incorporated ^{123}I/NIS imaging with ^{131}I radiation therapy to induce cytoreductive killing of tumor cells by radiation therapy. Timing is important in such radiovirotherapy studies; radiation therapy should be applied during the peak of NIS expression as measured from ^{123}I dosimetry measurements. It is also envisaged that, with better imaging equipment and more sensitive tracers,[37,38] one would also be able to track any off-target infection by the oncolytic viruses in clinical trials to facilitate better understanding of any off-target toxicity in the future. In conclusion, we have shown, for the first time, that VSV-mediated tumor infection and oncolytic activity can be monitored simultaneously with the combinatorial use of the NIS reporter gene and ^{99m}Tc-duramycin via SPECT/CT. This technique can be readily adapted to provide an early prognosis and reliable assessments of tumor responses to OV and is valuable in early-phase clinical development studies.

MATERIALS AND METHODS

Cell Culture and Viruses

MPC-11 and CT26 cell lines (American Type Cell Culture) were cultured in DMEM supplemented with 10% fetal bovine serum,

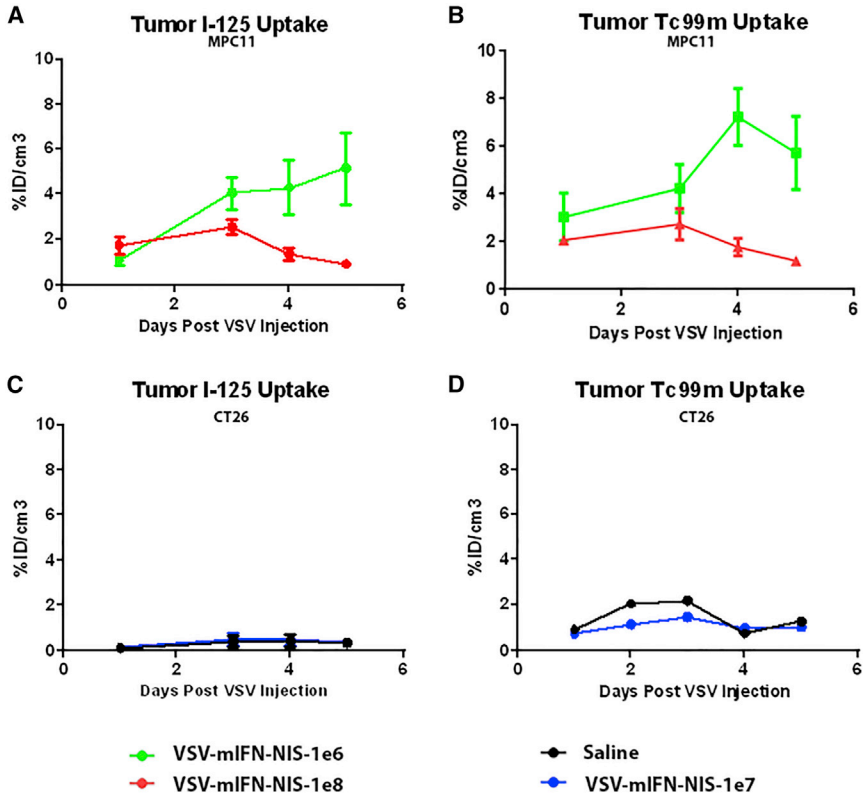

Figure 5. Correlation of VSV Infection (NIS-Mediated ^{125}I Uptake) and Cell Killing (^{99}Tc-Duramycin Uptake) with the Dose of VSV-mIFNβ-NIS Given Intravenously to BALB/c Mice

(A and B) ^{125}I uptake (A) or ^{99m}Tc uptake (B) in MPC-11 tumors of mice treated with 10^6 (green, four mice) or 10^8 (red, four mice) $TCID_{50}$ VSV-mIFNβ-NIS. (C and D) ^{125}I uptake (C) or ^{99m}Tc uptake (D) in CT26 tumors of mice treated with 10^7 $TCID_{50}$ VSV-mIFNβ-NIS (blue, four mice) or saline (black, two mice). Data are measured as the collective mean %ID/cm^3 for each model. Error bars denote SD associated with each data point.

100 U/mL penicillin, and 100 mg/mL streptomycin. Cell lines tested negative for mycoplasma contamination. The generation and propagation of VSV-mIFNβ-NIS have been previously described.[9]

Animals

Animals were maintained and cared for according to the guidelines of Mayo Clinic's Institutional Animal Care and Use Committee. Sixteen female BALB/c mice (Jackson Laboratory) aged 6–8 weeks were used in this study. A total of 5×10^6 MPC-11 cells or 5×10^6 CT26 cells were subcutaneously implanted in the right flank of the mice. When tumors reached 0.5 cm in diameter, VSV-mIFNβ-NIS was administered intravenously via the tail vein at a dose of 10^6, 10^7, or 10^8 $TCID_{50}$ per mouse. Saline injections were used as controls in both xenograft models. Mice were imaged under isoflurane inhalation anesthesia from day 2 post virus infusion.

Labeling Duramycin with ^{99m}Tc

Duramycin was labeled with ^{99m}Tc using tricine-phosphine coligands. The detailed procedure for the kit preparation has been described previously.[39] About 20 mCi ^{99m}Tc-pertechnetate in 500 μL of saline was added to the lyophilized vial. The labeling mixture was heated to 80°C in a lead-lined heating block for 20 min. The vial seal was vented with a 25G needle prior to removal from the heating block and was equilibrated to room temperature before injection.

SPECT/CT Imaging

One hour prior to SPECT/CT imaging, all MPC11- and CT26-bearing BALB/c mice received 300 μCi ^{125}I and 300 μCi ^{99m}Tc-duramycin (^{99m}Tc-duramycin) intravenously. Mice were imaged in a USPECT-II/CT scanner (MILabs, Utrecht, the Netherlands). CT was performed for 5 min, followed by SPECT, which simultaneously captured both ^{99m}Tc and ^{125}I signals. SPECT data were reconstructed using a standard ^{99m}Tc window and ^{125}I window, creating two distinct datasets. Window modes are described as follows: (1) ^{99m}Tc: 20% window, 140 keV (range 126–154 keV); (2) ^{125}I: 100% window, 30 keV (range 15–45 keV). Data processing and quantitation of ROI were performed by Imanis Life Sciences (Rochester, MN, USA) using PMOD software (Zurich, Switzerland).

Immunofluorescence and TUNEL Staining

Tumors were harvested at days 3 and 5 after SPECT imaging, fixed in 10% buffered formalin, followed by transfer to saline solution 3 days later. When radioactive material was no longer detectable, tumor specimens were embedded in paraffin and sectioned into 5-μm-thick slices. Immunohistochemical staining was performed using an anti-hNIS antibody (1:1,000, REA011; Imanis Life Sciences) or anti-VSV antibody (1:300, M2168; Mayo VVPL). TUNEL assays were performed on the serial section slices as per the manufacturer's instructions (G3250; Promega, Madison, WI, USA).

Data Analysis

SPECT data processing and quantitation of ROI were performed by Imanis Life Sciences (Rochester, MN, USA) using PMOD software (Zurich, Switzerland). GraphPad Prism (GraphPad Software, San Diego, CA, USA) was used for statistical calculations.

SUPPLEMENTAL INFORMATION

Supplemental Information can be found online at https://doi.org/10.1016/j.omto.2019.10.002.

AUTHOR CONTRIBUTIONS

Conception and design, S.J.R. and K.-W.P.; development of methodologies and performance of experiments, L.Z., L.S., M.Z., H.J., and T.R.D.; analysis and interpretation of data, L.Z. and L.S.; statistical analysis of data, L.Z. and L.S.; writing, review, and/or revision of the manuscript, L.Z., L.S, M.Z., S.J.R., and K.-W.P.; and study supervision, K.-W.P.

CONFLICTS OF INTEREST

S.J.R., K.-W.P., and Mayo Clinic have a financial interest in the technology used in this research. VSV and MV are licensed to Vyriad, and the NIS reporter gene technology is licensed to Imanis Life Sciences. L.S. is a full-time employee of Imanis.

ACKNOWLEDGMENTS

We thank Teresa Decklever and Dianna Glynn of the Mayo Clinic Nuclear Medicine Molecular Imaging Resource for their expert help in image acquisition. This study is supported by National Institutes of Health (R01 CA175795) and Mayo Foundation.

REFERENCES

1. Russell, S.J., Peng, K.W., and Bell, J.C. (2012). Oncolytic virotherapy. Nat. Biotechnol. *30*, 658–670.
2. Lawler, S.E., Speranza, M.C., Cho, C.F., and Chiocca, E.A. (2017). Oncolytic Viruses in Cancer Treatment: A Review. JAMA Oncol. *3*, 841–849.
3. Russell, L., and Peng, K.W. (2018). The emerging role of oncolytic virus therapy against cancer. Linchuang Zhongliuxue Zazhi *7*, 16.
4. Seymour, L.W., and Fisher, K.D. (2016). Oncolytic viruses: finally delivering. Br. J. Cancer *114*, 357–361.
5. Pol, J.G., Lévesque, S., Workenhe, S.T., Gujar, S., Le Boeuf, F., Clements, D.R., Fahrner, J.E., Fend, L., Bell, J.C., Mossman, K.L., et al. (2018). Trial Watch: Oncolytic viro-immunotherapy of hematologic and solid tumors. Oncoimmunology *7*, e1503032.
6. de Graaf, J.F., de Vor, L., Fouchier, R.A.M., and van den Hoogen, B.G. (2018). Armed oncolytic viruses: A kick-start for anti-tumor immunity. Cytokine Growth Factor Rev. *41*, 28–39.
7. Galanis, E., Atherton, P.J., Maurer, M.J., Knutson, K.L., Dowdy, S.C., Cliby, W.A., Haluska, P., Jr., Long, H.J., Oberg, A., Aderca, I., et al. (2015). Oncolytic measles virus expressing the sodium iodide symporter to treat drug-resistant ovarian cancer. Cancer Res. *75*, 22–30.
8. Russell, S.J., Federspiel, M.J., Peng, K.W., Tong, C., Dingli, D., Morice, W.G., Lowe, V., O'Connor, M.K., Kyle, R.A., Leung, N., et al. (2014). Remission of disseminated cancer after systemic oncolytic virotherapy. Mayo Clin. Proc. *89*, 926–933.
9. Naik, S., Nace, R., Federspiel, M.J., Barber, G.N., Peng, K.W., and Russell, S.J. (2012). Curative one-shot systemic virotherapy in murine myeloma. Leukemia *26*, 1870–1878.
10. Melzer, M.K., Lopez-Martinez, A., and Altomonte, J. (2017). Oncolytic Vesicular Stomatitis Virus as a Viro-Immunotherapy: Defeating Cancer with a "Hammer" and "Anvil". Biomedicines *5*, E8.
11. Hastie, E., and Grdzelishvili, V.Z. (2012). Vesicular stomatitis virus as a flexible platform for oncolytic virotherapy against cancer. J. Gen. Virol. *93*, 2529–2545.
12. Westcott, M.M., Liu, J., Rajani, K., D'Agostino, R., Jr., Lyles, D.S., and Porosnicu, M. (2015). Interferon Beta and Interferon Alpha 2a Differentially Protect Head and Neck Cancer Cells from Vesicular Stomatitis Virus-Induced Oncolysis. J. Virol. *89*, 7944–7954.
13. Penheiter, A.R., Russell, S.J., and Carlson, S.K. (2012). The sodium iodide symporter (NIS) as an imaging reporter for gene, viral, and cell-based therapies. Curr. Gene Ther. *12*, 33–47.
14. Goel, A., Carlson, S.K., Classic, K.L., Greiner, S., Naik, S., Power, A.T., Bell, J.C., and Russell, S.J. (2007). Radioiodide imaging and radiovirotherapy of multiple myeloma using VSV(Delta51)-NIS, an attenuated vesicular stomatitis virus encoding the sodium iodide symporter gene. Blood *110*, 2342–2350.
15. Miller, A., Suksanpaisan, L., Naik, S., Nace, R., Federspiel, M., Peng, K.W., and Russell, S.J. (2014). Reporter gene imaging identifies intratumoral infection voids as a critical barrier to systemic oncolytic virus efficacy. Mol. Ther. Oncolytics *1*, 14005.
16. Dispenzieri, A., Tong, C., LaPlant, B., Lacy, M.Q., Laumann, K., Dingli, D., Zhou, Y., Federspiel, M.J., Gertz, M.A., Hayman, S., et al. (2017). Phase I trial of systemic administration of Edmonston strain of measles virus genetically engineered to express the sodium iodide symporter in patients with recurrent or refractory multiple myeloma. Leukemia *31*, 2791–2798.
17. Zhao, M., Li, Z., and Bugenhagen, S. (2008). 99mTc-labeled duramycin as a novel phosphatidylethanolamine-binding molecular probe. J. Nucl. Med. *49*, 1345–1352.
18. Emoto, K., Toyama-Sorimachi, N., Karasuyama, H., Inoue, K., and Umeda, M. (1997). Exposure of phosphatidylethanolamine on the surface of apoptotic cells. Exp. Cell Res. *232*, 430–434.
19. Dingli, D., Peng, K.W., Harvey, M.E., Greipp, P.R., O'Connor, M.K., Cattaneo, R., Morris, J.C., and Russell, S.J. (2004). Image-guided radiovirotherapy for multiple myeloma using a recombinant measles virus expressing the thyroidal sodium iodide symporter. Blood *103*, 1641–1646.
20. Zhang, L., Steele, M.B., Jenks, N., Grell, J., Behrens, M., Nace, R., Naik, S., Federspiel, M.J., Russell, S.J., and Peng, K.W. (2016). Robust Oncolytic Virotherapy Induces Tumor Lysis Syndrome and Associated Toxicities in the MPC-11 Plasmacytoma Model. Mol. Ther. *24*, 2109–2117.
21. Ammayappan, A., Peng, K.W., and Russell, S.J. (2013). Characteristics of oncolytic vesicular stomatitis virus displaying tumor-targeting ligands. J. Virol. *87*, 13543–13555.
22. Ammayappan, A., Russell, S.J., and Federspiel, M.J. (2016). Recombinant mumps virus as a cancer therapeutic agent. Mol. Ther. Oncolytics *3*, 16019.
23. Gaddy, D.F., and Lyles, D.S. (2005). Vesicular stomatitis viruses expressing wild-type or mutant M proteins activate apoptosis through distinct pathways. J. Virol. *79*, 4170–4179.
24. Delvaeye, T., Wyffels, L., Deleye, S., Lemeire, K., Gonçalves, A., Decrock, E., Staelens, S., Leybaert, L., Vandenabeele, P., and Krysko, D.V. (2018). Noninvasive Whole-Body Imaging of Phosphatidylethanolamine as a Cell Death Marker Using ^{99m}Tc-Duramycin During TNF-Induced SIRS. J. Nucl. Med. *59*, 1140–1145.
25. Elvas, F., Boddaert, J., Vangestel, C., Pak, K., Gray, B., Kumar-Singh, S., Staelens, S., Stroobants, S., and Wyffels, L. (2017). ^{99m}Tc-Duramycin SPECT Imaging of Early Tumor Response to Targeted Therapy: A Comparison with ^{18}F-FDG PET. J. Nucl. Med. *58*, 665–670.
26. Elvas, F., Vangestel, C., Rapic, S., Verhaeghe, J., Gray, B., Pak, K., Stroobants, S., Staelens, S., and Wyffels, L. (2015). Characterization of [(99m)Tc]Duramycin as a SPECT Imaging Agent for Early Assessment of Tumor Apoptosis. Mol. Imaging Biol. *17*, 838–847.
27. Hu, Y., Liu, G., Zhang, H., Li, Y., Gray, B.D., Pak, K.Y., Choi, H.S., Cheng, D., and Shi, H. (2018). A Comparison of [^{99}mTc]Duramycin and [^{99}mTc]Annexin V in SPECT/CT Imaging Atherosclerotic Plaques. Mol. Imaging Biol. *20*, 249–259.
28. Ruotsalainen, J.J., Kaikkonen, M.U., Niittykoski, M., Martikainen, M.W., Lemay, C.G., Cox, J., De Silva, N.S., Kus, A., Falls, T.J., Diallo, J.S., et al. (2015). Clonal variation in interferon response determines the outcome of oncolytic virotherapy in mouse CT26 colon carcinoma model. Gene Ther. *22*, 65–75.
29. Ghonime, M.G., and Cassady, K.A. (2018). Combination Therapy Using Ruxolitinib and Oncolytic HSV Renders Resistant MPNSTs Susceptible to Virotherapy. Cancer Immunol. Res. *6*, 1499–1510.
30. Escobar-Zarate, D., Liu, Y.P., Suksanpaisan, L., Russell, S.J., and Peng, K.W. (2013). Overcoming cancer cell resistance to VSV oncolysis with JAK1/2 inhibitors. Cancer Gene Ther. *20*, 582–589.
31. Dold, C., Rodriguez Urbiola, C., Wollmann, G., Egerer, L., Muik, A., Bellmann, L., Fiegl, H., Marth, C., Kimpel, J., and von Laer, D. (2016). Application of interferon modulators to overcome partial resistance of human ovarian cancers to VSV-GP oncolytic viral therapy. Mol. Ther. Oncolytics *3*, 16021.

32. Rameix-Welti, M.A., Le Goffic, R., Hervé, P.L., Sourimant, J., Rémot, A., Riffault, S., Yu, Q., Galloux, M., Gault, E., and Eléouët, J.F. (2014). Visualizing the replication of respiratory syncytial virus in cells and in living mice. Nat. Commun. *5*, 5104.

33. Mehle, A. (2015). Fiat Luc: Bioluminescence Imaging Reveals In Vivo Viral Replication Dynamics. PLoS Pathog. *11*, e1005081.

34. Vandergaast, R., Khongwichit, S., Jiang, H., DeGrado, T.R., Peng, K.-W., Smith, D.R., Russell, S.J., and Suksanpaisan, L. (2019). Enhanced noninvasive imaging of oncology models using the NIS reporter gene and bioluminescence imaging. Cancer Gene Ther. January 24. https://doi.org/10.1038/s41417-019-0081-2.

35. Haddad, D., and Fong, Y. (2015). Molecular imaging of oncolytic viral therapy. Mol. Ther. Oncolytics *1*, 14007.

36. Eidenschink, B., Trujillo, M.J., Oneal, M., Morris, J.C., Yamamoto, M., and Davydova, J. (2014). NIS-mediated radioiodine therapy and imaging for pancreatic cancer with oncolytic adenovirus. Mol. Ther. *22* (*Suppl 1*), S65.

37. Jiang, H., Bansal, A., Goyal, R., Peng, K.W., Russell, S.J., and DeGrado, T.R. (2018). Synthesis and evaluation of ^{18}F-hexafluorophosphate as a novel PET probe for imaging of sodium/iodide symporter in a murine C6-glioma tumor model. Bioorg. Med. Chem. *26*, 225–231.

38. Jiang, H., and DeGrado, T.R. (2018). [^{18}F]Tetrafluoroborate ([^{18}F]TFB) and its analogs for PET imaging of the sodium/iodide symporter. Theranostics *8*, 3918–3931.

39. Zhao, M., and Li, Z. (2012). A single-step kit formulation for the (99m)Tc-labeling of HYNIC-Duramycin. Nucl. Med. Biol. *39*, 1006–1011.